



**HAL**  
open science

## Mathematical modeling of adipocyte size distributions: identifiability and parameter estimation from rat data

Anne-Sophie Giacobbi, Leo Meyer, Magali Ribot, Romain Yvinec, Hedi Soula,  
Chloe Audebert

### ► To cite this version:

Anne-Sophie Giacobbi, Leo Meyer, Magali Ribot, Romain Yvinec, Hedi Soula, et al.. Mathematical modeling of adipocyte size distributions: identifiability and parameter estimation from rat data. 2023. hal-04141173v1

**HAL Id: hal-04141173**

**<https://hal.science/hal-04141173v1>**

Preprint submitted on 26 Jun 2023 (v1), last revised 25 Jan 2024 (v3)

**HAL** is a multi-disciplinary open access archive for the deposit and dissemination of scientific research documents, whether they are published or not. The documents may come from teaching and research institutions in France or abroad, or from public or private research centers.

L'archive ouverte pluridisciplinaire **HAL**, est destinée au dépôt et à la diffusion de documents scientifiques de niveau recherche, publiés ou non, émanant des établissements d'enseignement et de recherche français ou étrangers, des laboratoires publics ou privés.



Distributed under a Creative Commons Attribution - NonCommercial - ShareAlike 4.0 International License

# Mathematical modeling of adipocyte size distributions: identifiability and parameter estimation from rat data

Anne-Sophie Giacobbi<sup>1,\*</sup>, Leo Meyer<sup>2</sup>, Magali Ribot<sup>2</sup>,  
Romain Yvinec<sup>3,4</sup>, Hedi Soula<sup>5</sup>, Chloe Audebert<sup>1,6,\*\*</sup>

<sup>1</sup> Sorbonne Université, CNRS, Institut de Biologie Paris-Seine (IBPS), Laboratory of Computational and Quantitative Biology UMR 7238, 75005 Paris, France

<sup>2</sup> Institut Denis Poisson, Université d'Orléans, CNRS, Université de Tours, 45067 Orléans, France

<sup>3</sup> PRC, INRAE, CNRS, Université de Tours, 37380 Nouzilly, France

<sup>4</sup> Université Paris-Saclay, Inria, Centre Inria de Saclay, 91120 Palaiseau, France

<sup>5</sup> Nutriomics, La Pitié-Salpêtrière, Sorbonne Université, CNRS, 75013 Paris, France

<sup>6</sup> Sorbonne Université, CNRS, Université de Paris, Laboratoire Jacques-Louis Lions UMR 7598, 75005 Paris, France

\* anne-sophie.giacobbi@sorbonne-universite.fr

\*\* chloe.audebert@sorbonne-universite.fr

---

## 1 Abstract

2 Fat cells, called adipocytes, are designed to regulate energy homeostasis by storing  
3 energy in the form of lipids. Adipocyte size distribution is assumed to play a role in  
4 the development of obesity-related diseases. This population of cells that do not have  
5 a characteristic size, indeed a bimodal size distribution is observed in adipose tissue.  
6 We propose a model based on a partial differential equation to describe adipocyte  
7 size distribution. The model includes a description of the lipid fluxes and the cell  
8 size fluctuations and using a formulation of a stationary solution fast computation of  
9 bimodal distribution is achieved. We investigate the parameter identifiability and es-  
10 timate parameter values with CMA-ES algorithm. We first validate the procedure on  
11 synthetic data, then we estimate parameter values with experimental data of 32 rats.  
12 We discuss the estimated parameter values and their variability within the popula-  
13 tion, as well as the relation between estimated values and their biological significance.  
14 Finally, a sensitivity analysis is performed to specify the influence of parameters on

15 cell size distribution and explain the differences between the model and the mea-  
16 surements. The proposed framework enables the characterization of adipocyte size  
17 distribution with four parameters and can be easily adapted to measurements of cell  
18 size distribution in different health conditions.

19

20 *keywords: parameter estimation, adipocyte size distribution, parameter identifiability,*  
21 *partial differential equation*

---

## 22 1 Introduction

23 Pathologies related to obesity are characterized by an important accretion of adipose  
24 tissue which is mainly composed of adipose cells, called adipocytes. The adipocytes  
25 are designed to regulate energy homeostasis by storing energy in form of lipids. Dur-  
26 ing an excess of energy, adipocytes compensate with two mechanisms: hypertrophy  
27 (increase in size) and hyperplasia (increase in number)[7]. Adipocyte size variations  
28 are very large with radii ranging from  $10\mu\text{m}$  to more than  $100\mu\text{m}$ , corresponding to  
29 3 orders of magnitude in volume. In addition, cell size distribution among a tissue is  
30 not unimodal but presents two peaks: one for small adipocytes (radius below  $30\mu\text{m}$ )  
31 and one for large adipocytes (above  $80\mu\text{m}$ ) [18]. A bimodal distribution of cell sizes  
32 is striking. Indeed, most cells in the population are small adipocytes, which do not  
33 contribute significantly to the storing capacity. There is no scientific consensus on the  
34 functional importance of this bimodality. However, cell size has been associated with  
35 metabolic properties dysfunction that may be linked to obesity-related pathologies  
36 [27, 22, 18, 16] or to play a role in the development of those diseases [5].

37 Few mathematical models have been proposed for adipocyte size dynamics in var-  
38 ious health conditions. In [12, 13, 14, 15], the authors consider partial differential  
39 equation models that describe adipocyte size distribution dynamics. They have as-  
40 sumed a size-dependent rate described by an imposed function where the associated  
41 parameters are difficult to relate to physiological processes. The adipocyte modeling  
42 in [17] is based on three compartments and has been developed to describe small,  
43 medium and large adipocytes. The cell size evolution depends on lipid fluxes that are  
44 related to protein concentration controlling lipotoxicity – a cellular dysfunction due  
45 to lipid accumulation in non-adipose tissue. All these models provide studies of the  
46 adipose tissue growth dynamic and its bimodality through cell hyperplasia and/or  
47 hypertrophy, but the mechanisms governing lipid fluxes involved in adipocyte hy-  
48 pertrophy have not been considered. Furthermore, model parameters lack biological  
49 meaning.

50 A detailed model of cell hypertrophy based on lipid exchanges has been proposed

51 in [24]. Adipocyte bimodal distributions have been explained based on mathemati-  
 52 cal analyses. Individual-based Monte Carlo techniques were performed to solve the  
 53 model. However, this approach is computationally costly so parameter estimation  
 54 using biological measurements is very difficult. A similar simplified model, accounting  
 55 only for lipolysis (deflation), compares well with distributions obtained from fasting  
 56 rats [25].

57 The paper is organized as follows. Based on [24, 25], we formulate the mathe-  
 58 matical model in section 2. It is based on partial differential equations, to describe  
 59 stationary adipocyte size distribution. The contribution of our work is to have a  
 60 diffusion term in the partial differential equation describing the cell size fluctuations  
 61 like in [13]. Through parameter estimation, we aim at comparing the distribution  
 62 obtained with the model to cell size distribution measured in rats before any manip-  
 63 ulation [25, 11]. To perform parameter estimation, we first conduct an identifiability  
 64 analysis in order to select model parameters that can be uniquely estimated with the  
 65 available data. Using these selected parameters, we carry out a study on synthetic  
 66 data (generated with model equations). The model identifiability and the parameter  
 67 estimation on synthetic data are presented in section 3. Once the parameter estima-  
 68 tion problem is verified, in section 4 we perform parameter estimation using adipocyte  
 69 size distributions measured in 32 healthy rats [25, 11]. The estimated parameters are  
 70 presented and then commented through a sensitivity analysis. We conclude this paper  
 71 with some discussions in section 5.

## 72 **2 Mathematical model for adipocyte size distribu-** 73 **tions**

### 74 **2.1 Model construction**

Based on Soula *et al.* [24] work, we introduce a new model for adipocyte size distri-  
 bution that we aim at fitting on experimental measurements. We first briefly recall  
 the main hypotheses of the model in [24]. To represent adipocyte size density, the  
 variation of the content of lipids  $\ell$  and variation of radius  $r$  to adapt to lipid content  
 are described by,

$$\left\{ \begin{array}{l} \frac{d\ell}{dt} = \mathcal{T}(r, \ell, L(t)), \\ \frac{dr}{dt} = \mathcal{R}(r, \ell), \end{array} \right. \quad (1) \quad (2)$$

75 where the term  $L(t)$  represents the extracellular amount of lipids at time  $t$ . These  
 76 two equations refer to evolution with different characteristic times: the first equation

77 is a rapid evolution of fatty acid content whereas the second is a slower variation of  
 78 radius to adapt to cell lipid content.

79 We first assume a quasi steady state for equation (2) to describe a faster adaptation  
 80 to lipid content. The relation between the lipid content  $\ell$  and the radius  $r$  of a cell is  
 81 then given by  $\mathcal{R}(r, \ell) = 0$ , leading to

$$\ell = \frac{V(r) - V_{em}}{V_\ell}, \quad V(r) = \frac{4}{3}\pi r^3, \quad (3)$$

82 with  $V_{em}$  the volume of the cell with no lipid,  $V_\ell$  the conversion constant: the volume  
 83 taken by 1 *nmol* of triglyceride, and the cell volume  $V(r)$  is assumed to be spherical.  
 84 Second, similarly to [13], we introduce a constant diffusion term  $D$  to represent cell  
 85 size fluctuations.

86 With the above mentioned assumptions, we can re-write the main equation in  
 87 [24], replacing  $\ell$  by (3) and keeping only the radius variable. We then consider the  
 88 cell size density  $f$  expressed as a function of time  $t \in \mathbb{R}_+$  and radius  $r \in [r_{min}, r_{max}]$ ,  
 89 and we introduce the following system:

$$\begin{cases} \partial_t f(t, r) + \partial_r(v(r, L(t))f(t, r)) - D\partial_r^2 f(t, r) = 0, & (4) \\ L(t) = \lambda - \int_{r_{min}}^{r_{max}} (V(r) - V_{em}) \frac{4\pi r^2}{V_\ell^2} f(t, r) dr, & (5) \\ v(r_{min}, L(t))f(t, r_{min}) - D\partial_r f(t, r_{min}) = 0, & (6) \\ v(r_{max}, L(t))f(t, r_{max}) - D\partial_r f(t, r_{max}) = 0, & (7) \end{cases}$$

90 where  $v$  is defined by

$$v(r, L) = \frac{V_\ell}{4\pi} \left( \alpha \frac{L}{L + \kappa} \frac{\rho^3}{\rho^3 + r^3} - \frac{(\beta + \gamma r^2)}{r^2} \frac{V(r) - V_{em}}{V(r) - V_{em} + V_\ell \chi} \right). \quad (8)$$

91 The total amount of lipids  $\lambda$  is assumed to be constant over time and the second  
 92 term of the right-hand side of (5) describes the intracellular amount of lipids at  
 93 time  $t$  contained within all cells. The transport function  $v$  describes the exchange  
 94 of lipids within the population of cells [24]. The lipid exchanges are based on two  
 95 biochemical processes: lipogenesis – cell store lipids – and lipolysis – release of lipids in  
 96 the extracellular environment. Lipogenesis depends on a surface-limited rate  $\alpha$ , and it  
 97 increases with the extracellular amount of lipids  $L$  with a saturation effect depending  
 98 on the value of  $\kappa$ . The parameter  $\rho$  is a cell size threshold above which lipogenesis  
 99 slows down. Lipolysis activity includes a basal rate  $\beta$  and a surface-limited rate  $\gamma$ .  
 100 The term  $\frac{V(r) - V_{em}}{V(r) - V_{em} + V_\ell \chi} = \frac{\ell}{\ell + \chi}$  is small when cells contain few lipids and becomes close  
 101 to one for larger lipid content through parameter  $\chi$ .

102 We assume that in the measurements at the time of the biopsy the adipose tissue  
 103 is at equilibrium, thus we neglect the recruitment of new cells. In addition, it has  
 104 been shown that the life time of a human adipocyte is around 10 years [2], so the cell  
 105 death is not taken into account. It gives the boundary conditions (6)-(7). The total  
 106 number of cells is then constant and we assume the density integral is 1 between  $r_{min}$   
 107 and  $r_{max}$ , which leads to

$$\forall t \geq 0, \int_{r_{min}}^{r_{max}} f(t, r) dr = 1. \quad (9)$$

108 Table 1 reports the details on model variables and parameters. The parameter  
 109 values of  $V_{em}$ ,  $V_l$ ,  $\beta$  and  $\gamma$  are known from literature [24, 25] and will be fixed. We  
 110 choose the values of  $r_{min}$  and  $r_{max}$  as the boundary values of the measured radii in  
 111 the considered adipose tissue.

## 112 2.2 Stationary solution

113 In model (4)-(7), the number of adipocytes is fixed and the total amount of lipids  
 114 is constant, thus we expect the size distribution to reach a steady state [21]. The  
 115 mathematical study of the asymptotic behavior is not the purpose of this work.

116 We denote by  $f^\infty$  and  $L^\infty$  a stationary density of cell size and the extracellular  
 117 amount of lipids respectively. A stationary solution verifies  $\partial_t f^\infty(r) = 0$ . With the  
 118 boundary conditions (6)-(7) and assuming  $D \neq 0$ , we obtain the following system:

$$\left\{ \begin{array}{l} \partial_r f^\infty(r) = \frac{1}{D} v(r, L^\infty) f^\infty(r), \end{array} \right. \quad (10)$$

$$\left\{ \begin{array}{l} L^\infty = \lambda - \int_{r_{min}}^{r_{max}} (V(r) - V_{em}) \frac{4\pi r^2}{V_\ell^2} f^\infty(r) dr. \end{array} \right. \quad (11)$$

119 We note that assuming  $f^\infty(r)$  is known for all  $r \in [r_{min}, r_{max}]$ , then  $L^\infty$  is de-  
 120 termined by the equation (11) and only depends on the unknown parameter  $\lambda$ . In  
 121 parameter identifiability analysis and parameter estimation we assume that the cell  
 122 size distribution is observed. So to simplify the dependency on parameters we con-  
 123 sider  $L$  to be a parameter instead of  $\lambda$ . We thus replace  $L^\infty$  by a parameter  $L$ , and  
 124 it leads to the following simplified model,

$$\left\{ \begin{array}{l} (f^\infty)'(r) = \frac{1}{D} v(r) f^\infty(r), \end{array} \right. \quad (12)$$

$$\left\{ \begin{array}{l} \int_{r_{min}}^{r_{max}} f^\infty(r) dr = 1, \end{array} \right. \quad (13)$$

$$\left\{ \begin{array}{l} v(r) = \frac{V_\ell}{4\pi} \left( \alpha \frac{L}{L + \kappa \rho^3 + r^3} - \frac{(\beta + \gamma r^2)}{r^2} \frac{V(r) - V_{em}}{V(r) - V_{em} + V_\ell \chi} \right), \end{array} \right. \quad (14)$$

Table 1: **Description of model variables and parameters.** Parameter units and known values are summed up in the second column and a description of each variable is given in the third column.

name	value (unit)	description
$t$	- ( $h$ )	time
$r$	$\in [7.5, 150]$ ( $\mu m$ )	adipocyte radius [25, 11]
$L(t)$	- ( $nmol$ )	extracellular amount of lipids at time $t$
$f(t, r)$	-	cell density at time $t$ with respect to radius $r$
$V_{em}$	$\frac{4\pi}{3} 6^3$ ( $\mu m^3$ )	volume of an empty adipocyte (zero lipid) [1]
$V_\ell$	$1.091 \cdot 10^6$ ( $\mu m^3 \cdot nmol^{-1}$ )	volume taken by 1 $nmol$ of triglyceride [24]
$\alpha$	- ( $nmol \cdot \mu m^{-2} \cdot h^{-1}$ )	surface-limited rate in lipogenesis
$\kappa$	- ( $nmol$ )	constant of the limiting term in lipogenesis
$\rho$	- ( $\mu m$ )	cell size threshold of the Hill function in lipogenesis
$\beta$	$31.25$ ( $nmol \cdot h^{-1}$ )	basal lipolysis rate [25]
$\gamma$	$0.27$ ( $nmol \cdot \mu m^{-2} \cdot h^{-1}$ )	surface-limited rate in lipolysis [25]
$\chi$	- ( $nmol$ )	constant of the limiting term in lipolysis
$D$	- ( $\mu m^2 \cdot h^{-1}$ )	diffusion coefficient for size fluctuations
$\lambda$	- ( $nmol$ )	total amount of lipids

125 where the unknown parameters to be estimated are  $\alpha$ ,  $L$ ,  $\kappa$ ,  $\rho$ ,  $\chi$  and  $D$ .

126 Given those parameters, we can compute a stationnary solution of model (12)-(14)  
 127 and we have for  $r \in [r_{min}, r_{max}]$ ,

$$f(r) = \frac{\exp\left(\int_{r_{min}}^r \frac{1}{D} v(s) ds\right)}{\int_{r_{min}}^{r_{max}} \exp\left(\int_{r_{min}}^r \frac{1}{D} v(s) ds\right) dr}. \quad (15)$$

128 This solution can be computed numerically and when possible, the integrals are com-  
 129 puted explicitly otherwise a trapezoid rule is used. Typically, in the computation, a  
 130 radius step of  $0.1 \mu m$  is considered and an interpolation is applied to compute  $f$  at  
 131 any radius.

### 132 **2.3 The model can represent a bimodal distribution of cell** 133 **size**

134 We first study the impact of the diffusion parameter that is the main change with  
 135 respect to model in [24]. Figure 1 shows solutions computed numerically with the

136 equation (15) for a given set of parameters. The model is able to qualitatively re-  
137 produce a bimodal distribution of cell size as measured in rats. Upon investigation  
138 of equations (12)-(14), it is immediate that the number of extremal points of  $f$ , and  
139 their locations, will depend only on the parameters that appear in the velocity  $v$  (14).  
140 However, variations in the value of the diffusion parameter also impact the size dis-  
141 tribution: increasing the diffusion reduces the difference between the height of the  
142 two peaks and the density value at the nadir (lowest point between the two peaks)  
143 increases with diffusion.

144 In the model of Soula et al. [24], an individual-based Monte Carlo technique  
145 (20,000 cells) has been performed leading to a large computational time. It was then  
146 very hard to perform quantitative comparison with measurements. The proposed  
147 model enables a fast computation of the cell size distribution by computing directly  
148 a stationary solution with equation (15). It is now possible to perform quantitative  
149 comparison with measured size distribution and estimate parameters.

150 Prior to this parameter estimation, we study which parameters are likely to be  
151 estimated with the available data through model parameter identifiability analysis  
152 and parameter estimation on synthetic data.

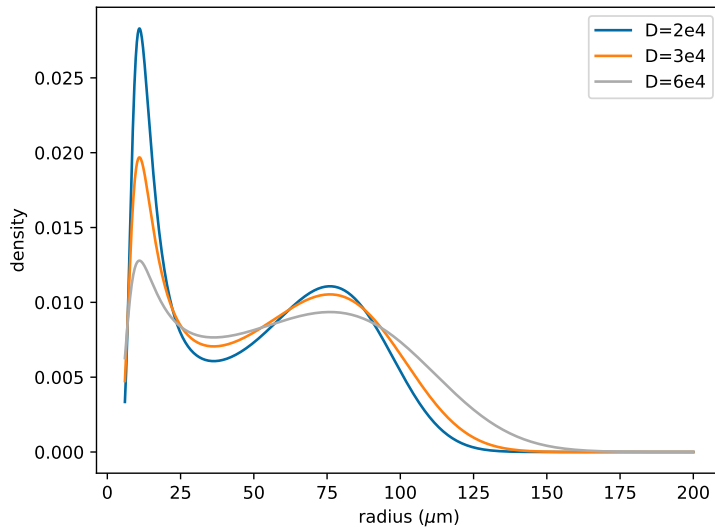


Figure 1: **Computed stationary solutions** from eq. 15 with three values for diffusion parameter. The other parameters are fixed to values reported in Table 1 and  $L = 3 \text{ nmol}$ ,  $\alpha = 0.29 \text{ nmol} \cdot \mu\text{m}^{-2} \cdot \text{h}^{-1}$ ,  $\kappa = 0.001 \text{ nmol}$ ,  $\rho = 200 \mu\text{m}$ ,  $\chi = 0.0035 \text{ nmol}$ .



### 3 Model identifiability and parameter estimation

#### 3.1 Parameter identifiability analysis

We perform an identifiability analysis of the unknown parameters of the model:  $\alpha$ ,  $L$ ,  $\kappa$ ,  $\rho$ ,  $\chi$  and  $D$ . We define a parameterized model  $\mathcal{M}(\theta)$  derived from equations (12)-(14) and study its parameter identifiability which is an intrinsic property: from [6], the model  $\mathcal{M}$  is said to be globally identifiable in  $\theta \in \Theta$  if

$$\forall \tilde{\theta} \in \Theta, \mathcal{M}(\theta) = \mathcal{M}(\tilde{\theta}) \Rightarrow \theta = \tilde{\theta}.$$

The parametric structure of model (12)-(14) is complex in the sense that it includes non-linear functions in which some parameters are combined in a product. This might result in redundancies in the model – only a smaller set of unknown parameters can be estimated – or in a non-identifiable model [4].

To study the parametric structure of the model, we first set the observed outputs,

$$x_1 = f^\infty, x_2 = r$$

and we introduce the following quantities to re-parameterize the model:

$$\theta_1 = \frac{\alpha L}{\beta(L + \kappa)}, \theta_2 = \rho^3, \theta_3 = V_\ell \chi \text{ and } \theta_4 = \frac{4\pi D}{V_\ell \beta}. \quad (16)$$

We obtain the system parameterized by  $\theta = (\theta_1, \theta_2, \theta_3, \theta_4)$  the vector of unknown quantities (assumed to be strictly positive),

$$\begin{cases} \frac{dx_1}{dr} = \frac{1}{\theta_4} \left( \theta_1 \frac{1}{1 + \frac{x_2^3}{\theta_2}} - \frac{1 + \frac{\gamma}{\beta} x_2^2}{x_2^2} \frac{\frac{4}{3}\pi x_2^3 - V_{em}}{\frac{4}{3}\pi x_2^3 - V_{em} + \theta_3} \right) x_1, \\ \frac{dx_2}{dr} = 1. \end{cases} \quad (17)$$

We recall that the values of  $V_{em}$ ,  $\beta$  and  $\gamma$  are known (see Table 1).

We investigate the identifiability of unknown parameters using the **Structural identifiability Toolbox** of Maple [28]. It is based on the Structural Identifiability ANalyser (SIAN) algorithm which combines differential algebra and Taylor series approaches [9, 10]. From an input ODE model, a polynomial equations system is generated and the associated Gröbner basis is computed to assess the identifiability. This method ranks parameters in three categories: *globally identifiable*, *locally but not globally identifiable* and *non-identifiable*. A parameter  $\theta_k$  is said to be locally identifiable if there is a finite set of possible values for  $\theta_k$  given the observation. When a parameter is neither locally nor globally identifiable, it is called non-identifiable.

Applied to the system (17), SIAN algorithm returns that all the quantities  $\theta_k, k \in \{1, \dots, 4\}$  are globally identifiable. Going back to the model parameters in equations (12)-(14), the parameters  $V_\ell, \beta$  are known and the function  $\rho \mapsto \rho^3$  is bijective so assuming the cell size distribution is observed, the set of identifiable quantities is

$$\left\{ \frac{\alpha L}{L + \kappa}, \rho, \chi, D \right\}.$$

172 We notice that we need at least the values of  $(L, \kappa)$ ,  $(L, \alpha)$  or  $(\alpha, \kappa)$  to uniquely  
 173 estimate  $\alpha, \kappa$  or  $L$  respectively. Only a combination of these values can be uniquely  
 174 retrieved when a size distribution  $f(r)$  is given for all  $r \in [r_{min}, r_{max}]$ .

### 175 3.2 Parameter estimation procedure

176 Thanks to the parameter identifiability analysis, we know which parameters or pa-  
 177 rameter combinations we can expect to estimate from size distribution. We now need  
 178 a procedure to estimate these parameters and we want to verify this procedure on a  
 179 benchmark case: synthetic data.

180 **Minimization algorithm** To define a procedure to estimate model parameters,  
 181 we first introduce a cost function. We want to minimize this function to compare the  
 182 model output and the measurements. Then, we choose an algorithm to minimize this  
 183 function.

184 Let  $\theta$  be the parameter vector to be estimated. We denote by  $N$  the number of  
 185 measured radii for the considered observation. Given the vector of measured radii,  
 186  $(r_i)_{i=1, \dots, N}$ , we estimate  $\theta$  by minimizing the cost function defined as follows,

$$\mathcal{L}(\theta) = - \sum_{i=1}^N \log(f(r_i, \theta)) \quad (18)$$

187 where  $f(r_i, \theta)$  is the value of a density  $f$ , solution of the model, computed at (mea-  
 188 sured) radius  $r_i$  with the parameter vector  $\theta$ .

189 To find the optimal parameter values, we use the Covariance Matrix Adaptation  
 190 Estimation Strategy (CMA-ES) algorithm [8]. In this algorithm, from initial parame-  
 191 ters, new possible solutions are sampled with a multivariate normal distribution. The  
 192 covariance matrix depends on a step-size control introduced to enhance the explo-  
 193 ration of parameter space. A weighted combination of the best candidates is then  
 194 selected according to the value of the cost function (18) and it is updated with the  
 195 covariance matrix. These steps are repeated until termination criteria are reached.  
 196 At each generation, this method takes into account recombination, mutation and  
 197 selection of the possible candidates as an evolution algorithm.

198 Estimation of  $(\theta_1, \rho, \theta_3, \theta_4)$  is performed with CMA-ES using cell size distribution  
 199 as observation (we replace  $\theta_2 = \rho^3$  by  $\rho$ ). The vector of parameters is also scaled to  
 200 have components of similar order of magnitude (scaling factors are  $[\theta_1 10^2, \rho 10^{-3}, \theta_3 10^{-4}, \theta_4 10^2]$ ).  
 201 Finally, to test the impact of the initial guess on the algorithm results, we perform 100  
 202 runs of CMA-ES with different initial parameters, we report the mean and standard  
 203 deviation of these runs.

204 In order to run the CMA-ES algorithm, we used `cma` Python package [29]. The  
 205 `fmin2` function of this package is used with default parameters and an initial standard  
 206 deviation of 0.05 (in each coordinate). The files to run parameter estimation are avail-  
 207 able on [https://plmlab.math.cnrs.fr/audebert/adipocyte\\_size\\_modeling](https://plmlab.math.cnrs.fr/audebert/adipocyte_size_modeling).

208 **Parameter estimation on synthetic data** We first estimate parameters with  
 209 data generated with the model (synthetic data). To generate such data, we compute  
 210 the solution of the model for chosen parameters with equation (15). Then, from  
 211 the obtained density, 10,000 samples are drawn leading to a first synthetic data set.  
 212 To mimic the true measurements we also consider a second type of synthetic data  
 213 where on the 10,000 samples only radii greater than  $10\mu m$  are observed. With this  
 214 procedure, we want to assess the impact of missing data on the parameter estimation.  
 215 To quantify the precision of the parameter estimation we compute a relative error  
 216 defined by  $\mathcal{E} = |p - p_e|/p$ , with  $p_e$  the parameter estimated value and  $p$  the true value  
 217 of the parameter (chosen to generate synthetic data).

218 Two different parameter vectors are used to obtain synthetic data sets (*synthetic*  
 219 *data set 1* and *synthetic data set 2*). The second column of Table 2 sums up the  
 220 chosen parameter values (true). The parameter estimation is performed for both  
 221 synthetic data sets without and with missing observations (Table 2 columns 3 to 8).

222 Columns 3 and 4 in Table 2 display the average and the standard deviation of the  
 223 estimated parameter values over the 100 runs. We note that the differences between  
 224 the 100 estimations can be neglected, showing that the initial guess has no impact on  
 225 the estimation.

226 In both synthetic data cases, when the estimation is performed with the complete  
 227 data set, the estimated parameter values are similar to the true values with relative  
 228 errors smaller than 5% (Table 2 column 5).

229 One can notice a difference between the two data sets when the estimation is  
 230 performed with missing observations in the data. The last three columns of Table  
 231 2 show that depending on the considered data set more or less information is lost  
 232 when we observe only cells with radii larger than a threshold. In *synthetic data set 1*,  
 233 the impact on the parameter estimation is relatively small and relative errors remain  
 234 below 5%. In *synthetic data set 2*, we are able to correctly estimate the values of  $\theta_1$ ,  
 235  $\rho$  and  $\theta_4$  but the information about parameter  $\theta_3$  seems lost, and the relative error

Table 2: **Results of parameter estimation procedure performed on synthetic data sets without and with missing data.** First two columns display the parameter names and true values for both synthetic data sets. Columns 3 and 4 present the estimated parameters for complete data sets (10,000 samples), it shows the average over 100 estimations with different initial guesses and standard deviations. The fifth column sums up the difference between true parameter and its estimation with a relative error in percentage. The three last columns present the same values for the same data sets with missing observations: only radii over  $10\mu m$  are observed (samples  $> 10\mu m$ ). All estimations are performed with CMA-ES algorithm of `fmin2` function from `cma` Python package. We choose the default parameters and an initial standard deviation of 0.05 (in each coordinate). The parameters are scaled to have similar sensitivity ( $[\theta_1 \cdot 10^2, \rho \cdot 10^{-3}, \theta_3 \cdot 10^{-4}, \theta_4 \cdot 10^2]$ ).

<i>synthetic data set 1</i>		10,000 samples			samples $> 10\mu m$		
parameter	true	esti. value	std	rel. err.	esti. value	std	rel. err.
$\theta_1$	$9.60 \cdot 10^{-3}$	$9.61 \cdot 10^{-3}$	$1 \cdot 10^{-11}$	0.2%	$9.62 \cdot 10^{-3}$	$2 \cdot 10^{-11}$	0.3%
$\rho$	$1.50 \cdot 10^2$	$1.50 \cdot 10^2$	$1 \cdot 10^{-6}$	0.2%	$1.49 \cdot 10^2$	$2 \cdot 10^{-6}$	0.8%
$\theta_3$	$2.18 \cdot 10^3$	$2.17 \cdot 10^3$	$5 \cdot 10^{-5}$	0.6%	$2.09 \cdot 10^3$	$2 \cdot 10^{-4}$	4.2%
$\theta_4$	$7.37 \cdot 10^{-3}$	$7.2 \cdot 10^{-3}$	$2 \cdot 10^{-10}$	2.3%	$7.35 \cdot 10^{-3}$	$4 \cdot 10^{-10}$	0.3%
<i>synthetic data set 2</i>		10,000 samples			samples $> 10\mu m$		
parameter	true	esti. value	std	rel. err.	esti. value	std	rel. err.
$\theta_1$	$9.92 \cdot 10^{-3}$	$9.92 \cdot 10^{-3}$	$1 \cdot 10^{-11}$	0.04%	$9.91 \cdot 10^{-3}$	$1 \cdot 10^{-10}$	0.1%
$\rho$	$2.00 \cdot 10^2$	$2 \cdot 10^2$	$1 \cdot 10^{-6}$	0.2%	$2.01 \cdot 10^2$	$5 \cdot 10^{-6}$	0.6%
$\theta_3$	$3.27 \cdot 10^2$	$3.12 \cdot 10^2$	$2 \cdot 10^{-5}$	4.8%	$5.39 \cdot 10^2$	$4 \cdot 10^{-4}$	65%
$\theta_4$	$1.11 \cdot 10^{-2}$	$1.12 \cdot 10^{-2}$	$2 \cdot 10^{-10}$	1.7%	$1.12 \cdot 10^{-2}$	$1 \cdot 10^{-9}$	1.2%

236 increases to 65%.

237 The number of observed cells is reduced in these data sets and not in the same  
238 way in each set. On synthetic data we know exactly the percentage of information  
239 that is missing. In *synthetic data set 1* when we remove samples larger than  $10\mu m$ ,  
240 15% of the observation is missing, whereas in *synthetic data set 2* we remove 28%  
241 of the initial distribution. This difference may explain the poor estimation of  $\theta_3$  in  
242 *synthetic data set 2* with missing observations.

243 The parameter  $\theta_3$  is related to parameter  $\chi$  that drives the lipolysis mechanism  
244 in the model (size reduction). If limited observations exist on small radius, we can  
245 expect that this parameter is difficult to estimate.

246 **From estimated parameter values to parameter intervals** The identifiability  
247 analysis ensures that the minimization problem should have only one solution and  
248 the estimation procedure computes this solution. Here, we want to compute inter-

249 vals of parameter values for which the cost function remains close to its minimum.  
250 Our approach follows the strategy of ABC method where parameters are sampled  
251 from a prior distribution and are then selected according to a criterion based on the  
252 evaluation of the model output [26].

253 To sample a parameter  $\theta_i$ , a new parameter  $\bar{\theta}_i$  is first generated uniformly in  
254  $[0.8\hat{\theta}_i, 1.2\hat{\theta}_i]$  where  $\hat{\theta}_i$  is the estimated parameter value obtained with the CMA-ES  
255 algorithm. Then, the cost function is computed with parameter  $\bar{\theta}_i$  while the other  
256 parameters are fixed at their estimated values. The parameter is selected if the cost  
257 function is below 0.1% of  $\mathcal{L}(\hat{\theta})$ . This threshold was set to investigate the parameter  
258 space with small changes on cell size distribution. Note that the parameter sampling  
259 is performed one at a time. This strategy is repeated until 1,000 replicates are selected  
260 per parameter.

261 Table 3 shows for each parameter the considered range of values and the selected  
262 intervals for each synthetic data set. For synthetic data sets without missing obser-  
263 vations, the range of values selected by the procedure is reduced in comparison with  
264 the initial one and contains the true parameter. This analysis gives an information  
265 on the range of accepted values for each parameter. We note that, in *synthetic data*  
266 *set 1*, the model output seems less sensitive to parameter  $\theta_4$  that has the largest range  
267 of selected values. In *synthetic data set 2* the largest range of selected values is for  
268 parameter  $\theta_3$ .

269 In data sets with missing observations, the selected ranges are not impacted for  
270 *synthetic data set 1* (small difference for  $\theta_3$ ). In *synthetic data set 2*, the loss of  
271 information about small cells leads to the selection of the total initial interval for  
272 parameter  $\theta_3$  ( $\pm 20\%$  of the estimated value) and an important increase of the se-  
273 lected range for  $\theta_4$  (almost twice the length) compared to the case without missing  
274 observations. As observed in section 2.3, parameter  $D$  (hence  $\theta_4$ ) controls the rela-  
275 tive heights of both modes in the cell size distribution. This can explain that data  
276 sets with missing observations on small sizes lead to higher uncertainty on  $\theta_4$ . These  
277 results are in agreement with the computed relative errors of the previous paragraph  
278 (Table 2).

## 279 4 Application to adipocyte size distribution mea- 280 sured in rats

### 281 4.1 Measurements of adipocyte size distribution

282 The measured cell size distributions used to perform parameter estimation come from  
283 previous experiments [25] and data from [11], but this part of the experiment has  
284 not been published. Here, only adipocyte size distributions of animals in normal

Table 3: **Range of selected values for the parameters.** The first three columns show the parameter names, order and true value. For each data set, the estimated parameter value (column “esti. value”) with CMA-ES method is subject to a maximum of 20% variation (column “esti.  $\pm 20\%$ ”). From this variation, a range of values is selected for each parameter (column “selec. values”) allowing a maximum error rate of 0.1% on the value of the estimated cost function  $\mathcal{L}$ . For each parameter 1,000 samples are generated

<i>synthetic data set 1</i>			10,000 samples			samples $> 10\mu m$		
parameter	order	true	esti. value	esti. $\pm 20\%$	selec. values	esti. value	esti. $\pm 20\%$	selec. values
$\theta_1$	$10^{-3}$	9.60	9.61	7.69 - 11.53	9.58 - 9.63	9.62	7.70 - 11.54	9.59 - 9.65
$\rho$	$10^2$	1.50	1.50	1.20 - 1.80	1.47 - 1.53	1.49	1.19 - 1.79	1.46 - 1.52
$\theta_3$	$10^3$	2.18	2.17	1.74 - 2.60	2.05 - 2.29	2.09	1.67 - 2.51	1.91 - 2.29
$\theta_4$	$10^{-3}$	7.37	7.20	5.76 - 8.64	6.54 - 8.02	7.35	5.88 - 8.82	6.58 - 8.32
<i>synthetic data set 2</i>			10,000 samples			samples $> 10\mu m$		
parameter	order	true	esti. value	esti. $\pm 20\%$	selec. values	esti. value	esti. $\pm 20\%$	selec. values
$\theta_1$	$10^{-3}$	9.92	9.92	7.94 - 11.90	9.90 - 9.95	9.91	7.92 - 11.89	9.86 - 9.95
$\rho$	$10^2$	2.00	2.00	1.60 - 2.40	1.97 - 2.03	2.01	1.61 - 2.41	1.99 - 2.05
$\theta_3$	$10^3$	3.27	3.12	2.49 - 3.74	2.69 - 3.58	5.39	4.31 - 6.47	4.32 - 6.47
$\theta_4$	$10^{-2}$	1.11	1.12	0.90 - 1.34	1.05 - 1.21	1.12	0.90 - 1.34	0.98 - 1.28

285 physiological conditions are considered.

286 We use two data sets of size distribution in retroperitoneal adipose tissue for  
287 a total of 32 male Wistar rats (20 rats METAJ, aged between 20 and 24 months,  
288 Charles River, L’Arbresle, France and, 12 rats EMPA, 12-week-old, Le Genest-Saint-  
289 Isle, France). Cell size distributions were measured with Beckman Coulter Multisizer  
290 IV (Beckman Coulter, Villepinte, France) [18]. Due to limitation in measurement  
291 techniques, only cell radii larger than  $7.5\mu m$  for the first experiment and  $10\mu m$  in the  
292 second were measured. Each animal cell size distribution is composed of a minimum  
293 of 6,000 cell radii.

## 294 4.2 Parameter estimation with measured data

295 The estimation procedure validated on synthetic data is now applied to measured  
296 size distributions. Parameter estimation is performed with CMA-ES algorithm with  
297 radius distributions measured for 32 rats in the same experimental conditions. Fig-  
298 ure 2 shows four examples of model-data fitting (the model fitting results of the 32  
299 rats are available on [https://plmlab.math.cnrs.fr/audebert/adipocyte\\_size\\_](https://plmlab.math.cnrs.fr/audebert/adipocyte_size_modeling)  
300 [modeling](https://plmlab.math.cnrs.fr/audebert/adipocyte_size_modeling)). These results show the ability of the model to reproduce different types  
301 of cell size distribution. The height of each peak is not always correctly captured.  
302 This could be related to the loss of information due to missing observation for small  
303 cells in experimental data. In addition, the nadir is always underestimated by the

304 model. We hypothesize that we are missing a process in the model to properly cap-  
 305 ture this point. However, the overall size distribution obtained with the model is in  
 306 good agreement with the measured one.

307 Table 4 shows the mean, standard deviation and relative standard deviation (RSD)  
 308 of the estimated parameter values obtained in the 32 rats. The RSD are relatively  
 309 small for  $\theta_1$  and  $\rho$ , showing that the size distribution of adipocytes for rats in the  
 310 same experimental conditions can be characterized with parameters in the same value  
 311 ranges. The variability in the population is larger for parameter  $\theta_3$  and  $\theta_4$  (larger  
 312 RSD). However, the previous analysis on synthetic data showed that less confidence  
 313 in the estimation is expected for these parameters, especially  $\theta_3$ .

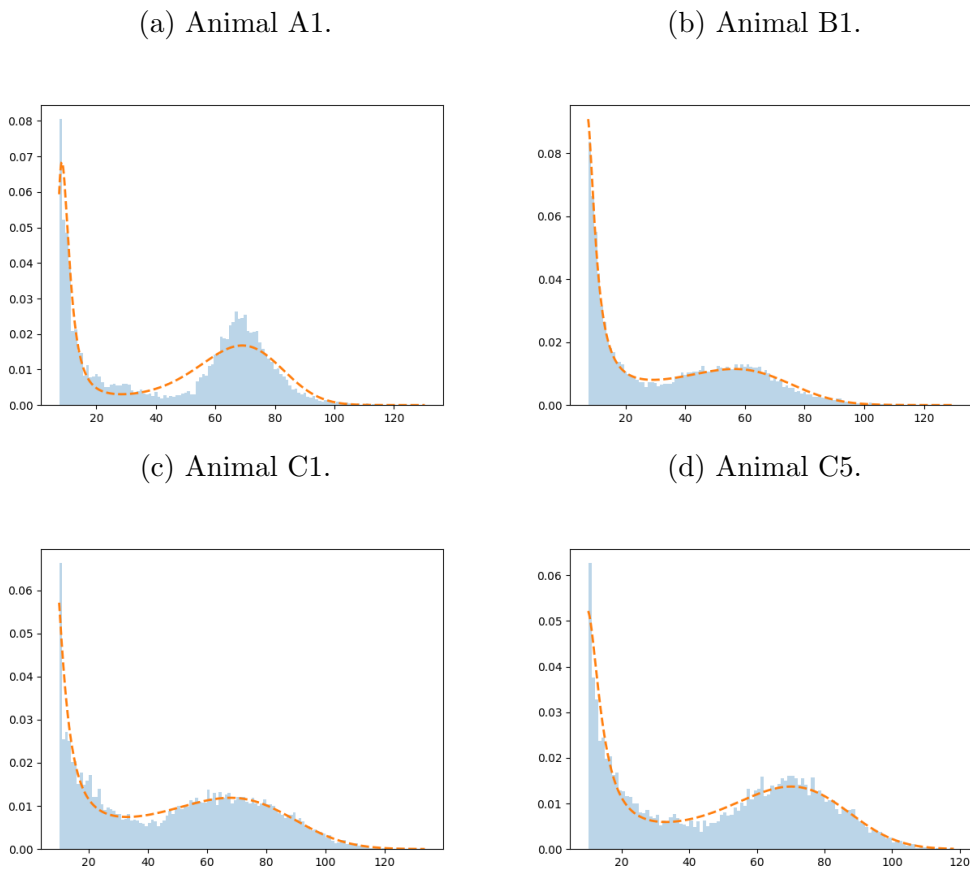


Figure 2: **Comparison model-data.** Four examples (over 32) of adipocyte radius distributions (in  $\mu m$ ) as histograms in rat in normal physiological conditions and model output computed (dash lines) with estimated parameters (see section 4.1). The parameter estimations are performed with CMA-ES algorithm of `cma` Python package by minimizing the function  $\mathcal{L}$  eq. 18.

Table 4: **Parameter estimation with adipocyte size distributions measured in rats.** The first column is the parameter names. Over 32 estimations with the different animal cell size distributions, the mean is presented in the second column, the standard deviation in the third column and the fourth column is the relative standard deviation *i.e* the ratio of standard deviation over mean. The parameters are estimated with CMA-ES algorithm of `fmin2` function from `cma` Python package (with 100 initial guesses).

parameters	mean	std	RSD
$\theta_1$	$9.6 \cdot 10^{-3}$	$2.8 \cdot 10^{-4}$	0.03
$\rho$	$1.57 \cdot 10^2$	$0.25 \cdot 10^2$	0.16
$\theta_3$	$2.24 \cdot 10^3$	$1.07 \cdot 10^3$	0.47
$\theta_4$	$8.21 \cdot 10^{-3}$	$2.58 \cdot 10^{-3}$	0.31

314 For each animal, accepted parameter ranges are also computed following the pro-  
315 cedure described in section 3.2 (Table 5). Figure 3 displays for each parameter the  
316 estimated value for each animal with the range of selected values (dots and bars).  
317 As expected, the parameter ranges are larger for parameters  $\theta_3$  and  $\theta_4$  compared to  
318 parameters  $\theta_1$  and  $\rho$ . Figure 3 also shows the mean (dash red line) and the standard  
319 deviation (gray area) over the rat population for each estimated parameter. It en-  
320 ables to compare the amplitude of the range of accepted values for each parameter  
321 for each animal with the variability within the population. We can see that for each  
322 parameter the range of accepted values is always smaller than the standard deviation  
323 in the population. It shows that the largest standard deviation within the population  
324 obtained for  $\theta_3$  and  $\theta_4$  (Table 4) should not be attributed to less confidence in the  
325 estimations.

326 The range of selected values of parameter  $\theta_3$  in rats population is between 1070 and  
327  $4429 \mu m^3$ . From this range of values, we can compute a range of radii for which the  
328 lipolysis term becomes mainly a surface based mechanism (i.e.  $(V(r) - V_{em}) / (V(r) -$   
329  $V_{em} + \theta_3) > 0.95$ ). We find radii in the range  $17.2 - 27.3 \mu m$ .

330 Similarly, for lipogenesis, the parameter  $\theta_1$  is estimated within the rats population  
331 between 0.0092 and  $0.010 \mu m^{-2}$ . We remind that this quantity is a combination of  
332 parameters :  $\theta_1 = \frac{\alpha L}{\beta(L+\kappa)}$  and parameter  $\beta$  is known [25]. We then obtain an esti-  
333 mation of  $\frac{\alpha L}{(L+\kappa)}$  between 0.29 and  $0.31 nmol.\mu m^{-2}.h^{-1}$ . In the case of high available  
334 lipids,  $L$  is large and we can assume  $\frac{L}{L+\kappa} \sim 1$ . Under this assumption, the parameter  
335  $\alpha$  is estimated between 0.29 and  $0.31 nmol.\mu m^{-2}.h^{-1}$ . An alternative case is for low  
336  $L$ , then we can assume  $\frac{L}{L+\kappa} \sim L$  and the estimated values of  $\theta_1$  provide an estimation  
337 for  $\alpha L$ .

338 The cell size threshold  $\rho$  of the Hill function in lipogenesis term is estimated in



339 the range  $115 - 204\mu m$ . Above this threshold, the term  $\rho^3/(\rho^3 + r^3)$  is smaller than  
340 0.5 and limits the growth of the cell.

### 341 4.3 Sensitivity analysis

342 In order to investigate the differences between model output and measured cell size  
343 distribution, a sensitivity analysis is performed. Sensitivity analysis is a local analysis  
344 and quantifies how sensitive the model output is to parameter changes. We choose to  
345 apply the Sobol' method [23]. The sensitivity indices are based on the decomposition  
346 of the output variance at each cell size point.

347 The first order index measures the singular effect of a parameter on the model  
348 output. It represents the contribution part of the parameter alone in the variability of  
349 model output. A high value of this index indicates a high contribution of the param-  
350 eter, which means that the model output is highly sensitive to this parameter. The  
351 total order index enables to include the effects depending on parameter interactions  
352 (higher order indices).

353 The model output is the cell size distribution  $f$  computed with equation (15) for  
354 radii from  $7.5\mu m$  to  $140\mu m$ . To study the influence of the estimated parameters, each  
355 parameter  $\theta_i$  is uniformly distributed in a range of  $\pm 1\%$  of estimated mean over the  
356 population of rats (Table 4). The change of  $\pm 1\%$  in parameters values is chosen such  
357 that the adipocyte size distributions computed with these parameters are bimodal.  
358 Then, Saltelli algorithm is performed to explore the parameter space leading to the  
359 generation of  $n(2d + 2)$  parameter samples with a Monte-Carlo approach [20, 23]. We  
360 choose  $n = 2048$  and  $d = 4$  the number of parameters. The sensitivity analysis is  
361 performed using the SALib Python Library [23, 20, 3, 19].

362 Figure 4(a) shows cell size distributions ranges computed with parameters from  
363 the sampling design. With these small perturbations, a large variability is found  
364 between the cell size distributions around the two modes. The first mode of the  
365 adipocyte size density is represented by cells with radii from  $7.5$  to  $10\mu m$ . Regarding  
366 large adipocytes, the higher densities present a high variability and correspond to  
367 adipocyte size values from  $50$  to  $120\mu m$ . These results illustrate the heterogeneity of  
368 cell sizes that can be obtained with the model with small changes in parameters.

369 Then, Sobol' indices are computed to determine which parameters are most influ-  
370 ential on the cell size dynamic. The first-order indices are displayed for several radii  
371 and each parameter in Figure 4(b). The results indicate that parameter  $\theta_1$  explains  
372 the most the variations of cell sizes with a first-order sensitivity index between 0.6  
373 and 1 for all radii. Interestingly, for the cells with radii around  $40\mu m$ , the index of  
374  $\theta_1$  decreases and we notice that  $\rho$  index increases (index equals 0.36). It shows that  
375 parameter  $\rho$  around this point explains the variability of the model output up to  
376 36%. The impacts of  $\theta_3$  and  $\theta_4$  are almost negligible on cells size distribution. From

377  $r = 90\mu m$ , the results show that the influence of  $\theta_1$  decreases whereas  $\rho$  becomes  
378 more influential and explains up to 18% of the output variability. The total-order  
379 sensitivity indices are also computed (not shown) and are similar to first-order indices,  
380 revealing that parameter interactions have a negligible influence on the adipocyte size  
381 distributions.

382 The sensitivity analysis suggests that the cell size dynamics in rats is mainly driven  
383 by the parameters depending on lipogenesis, and especially by  $\theta_1$  which represents  
384 the combination of the unknown parameters  $(\alpha, \kappa, L)$ .

385 Parameters  $\theta_3$  and  $\theta_4$ , associated with lipolysis (through  $\chi$ ) and diffusion ( $D$ )  
386 respectively, have a negligible impact on the cell size dynamic along all cell sizes.  
387 This result confirms the difficulty to identify these parameters in practice and are  
388 in agreement with the largest ranges of selected parameter values. In addition, this  
389 study highlights the fact that the nadir is difficult to capture since we observe an  
390 opposite change in the parameter sensitivity around this radius. With this study we  
391 are able to explain the results of parameter estimation on the measured data.

## 392 5 Discussion

393 We presented a mathematical model to describe adipocytes cell size distribution,  
394 based on a partial differential equation and including lipid exchanges. With the  
395 formulation of a stationary solution we were able to solve numerically and efficiently  
396 this model. Prior to the estimation of parameter with measurements we analyzed  
397 which parameter can be identifiable and how reliable are the estimations.

398 The identifiability of unknown parameters was studied with a re-parameterized  
399 form of the model. We showed that only four quantities can be uniquely identified  
400 and that three of our parameters of interest are related. These three parameters  
401 cannot be identified separately with an observation of the cell size distribution only.  
402 However, we can identify the threshold radius  $\rho$  involved in lipogenesis, the lipolysis  
403 threshold  $\chi$  as well as the diffusion coefficient  $D$  that describes cell size fluctuations.

404 The model calibration on synthetic data sets showed, in practice, an accurate  
405 estimation of the parameters. When we considered data sets with missing observations  
406 (similar to the measurements) we found that three over the four quantities can be  
407 correctly estimated.

408 The model parameters were estimated on 32 adipocyte size distributions measured  
409 in rats. With these estimated parameters, the overall distribution of cell size was  
410 captured. However, the nadir part of the distribution as well as the height of the  
411 modes were not perfectly reproduced. It is possible that the model is missing some  
412 aspect of the adipocyte size dynamics that would help to better capture the nadir.  
413 This is supported by the sensitivity analysis, that showed that the nadir part was not

414 sensitive specifically to one of the four considered parameters. Therefore, it makes  
415 this part of the distribution difficult to fit. In addition, in the presented model, the  
416 diffusion parameter  $D$  via  $\theta_4$  affects linearly both lipogenesis and lipolysis. It would  
417 be interesting to change this modeling assumption with a more complex diffusion  
418 process, impacting differently lipogenesis and lipolysis. For instance, considering a  
419 size dependent diffusion coefficient could improve the agreement between the model  
420 outputs and the observations.

421 We also think that our assumption regarding the normalization of the cell size  
422 distribution (it integrates to 1 between  $r_{min}$  and  $r_{max}$ ) affects the fits (especially  
423 the height of the 2 modes). However, we have no background knowledge about the  
424 total number of adipocytes in the distribution. In addition, we know that the data  
425 collection does not include cells with a radius below a certain threshold. In [12], a  
426 formulation has been proposed to approximate the total cell number in a fat pad  
427 but to do this estimation, we need to have the fat pad mass which is not the case  
428 in our experimental data. An other way to solve this issue would be to introduce  
429 a parameter that quantifies the total number of cells. However with an additional  
430 parameter, we will lose parameter identifiability. Then, we might need to fix other  
431 unknown quantities, so this solution only shifts the problem.

432 Nevertheless, we have estimated parameter values for 32 rats. We found a larger  
433 variability between rats in the estimated values of  $\theta_3$  and  $\theta_4$  (Figure 3). However,  
434 the sensitivity analysis showed that the model is less sensitive to these parameters  
435 (Figure 4). For  $\theta_1$  and  $\rho$ , the estimated values were more robust within the population  
436 leading us to believe that  $\theta_1$ ,  $\rho$  are less individual-specific parameters. However they  
437 could change if the estimation is performed with another species. This result sug-  
438 gests lipolysis (driven by  $\chi$ ) is more an individual-dependent process than lipogenesis  
439 (driven by  $\theta_1$  and  $\rho$ ) that is more constant within the population.

440 Recruitment of new cells via adipogenesis was not included in our model. Since  
441 we were looking at the distribution of size at one specific time, this mechanism can be  
442 neglected. However, if one wants to represent longitudinal adipocyte size distributions  
443 specially in case of diet changes, this process should be considered. This will have  
444 an impact on the cell size distribution, especially for small cells, as suggested in [25].  
445 Moreover, it is known that past diets affect the adipocyte size regulation and may  
446 be irreversible [12, 24]. Indeed, past diets could lead to a larger number of cells  
447 in the tissue. However, in the presented model, the number of cells is not explicitly  
448 considered. This assumption should be modified to take into account longitudinal size  
449 distributions and to be able to compare animals with different diets. In past works  
450 [12, 13, 14, 15], the authors have considered partial differential equation models that  
451 take into account a recruitment rate of new cells. Our model could be extended with  
452 this extra term for adipogenesis modeling.

453 We believe that the presented framework can be adapted to estimate model pa-

454 rameters with adipocyte size distribution in other species than rats and in different  
455 health conditions. It may enable to establish links between the mathematical model  
456 parameters and health conditions based on adipocyte size distribution observations.  
457 The final purpose is to be able to characterize and potentially classify the different  
458 obesity-related pathologies.

## 459 **6 Acknowledgments**

460 This work was supported the ANR MATIDY grant (ANR-20-CE45-0003).

## 461 **References**

- 462 [1] Alberts, B., Johnson, A., Lewis, J., Ra, M., Roberts, K., et al. (2002). *Molecular*  
463 *Biology of the Cell*, fourth edition, 197.
- 464 [2] Arner, E., Westermark, P. O., Spalding, K. L., Britton, T., Rydén, M., Frisé, J.,  
465 Bernard, S., Arner, P. (2010). Adipocyte turnover: relevance to human adipose  
466 tissue morphology. *Diabetes*, 59(1), 105–109. <https://doi.org/10.2337/db09-0942>
- 467 [3] Campolongo, F., Saltelli, A., Cariboni, J. (2011) From screening to quantitative  
468 sensitivity analysis. *Computer Physics Communications* 182,  
469 978–988. <https://doi.org/10.1016/j.cpc.2010.12.039>.
- 470 [4] Catchpole E. A., MORGAN B. J. T. (1997) Detecting parameter redundancy.  
471 *Biometrika*, 84(1), 187–196. <https://doi.org/10.1093/biomet/84.1.187>
- 472 [5] Clément, K. (2011). Bariatric surgery, adipose tissue and gut microbiota. *Int J*  
473 *Obes* 35 (Suppl 3), S7–S15. <https://doi.org/10.1038/ijo.2011.141>
- 474 [6] Cole D.J., Morgan B.J., Titterington D.M. (2010) Determining  
475 the parametric structure of models. *Math Biosci*, 228(1), 16-30.  
476 <https://doi.org/10.1016/j.mbs.2010.08.004>
- 477 [7] Drolet, R., Richard, C., Sniderman, A.D., Mailloux, J., Fortier, M., Huot,  
478 C., Rhéaume, C., Tchernof, A. (2008). Hypertrophy and hyperplasia of ab-  
479 dominal adipose tissues in women. *Int. J. Obes. (London)* 32 (2), 283–291.  
480 <http://dx.doi.org/10.1038/sj.ijo.0803708>
- 481 [8] Hansen, N. (2016). *The CMA Evolution Strategy : A Tutorial*.  
482 <https://doi.org/10.48550/arXiv.1604.00772>

- 483 [9] Hong H., Ovchinnikov A., Pogudin G., and Yap C. (2019) SIAN: software for  
484 structural identifiability analysis of ODE models. *Bioinformatics*, 35(16), 2873-  
485 2874. <https://doi.org/10.1093/bioinformatics/bty1069>
- 486 [10] Hong H., Ovchinnikov A., Pogudin G., and Yap C. (2020) Global identifiability  
487 of differential models. *Communications on pure and applied mathematics*, 73(9),  
488 1831–1879. <https://doi.org/10.1002/cpa.21921>
- 489 [11] Jacquier M., Crauste F., Soulage C.O., Soula H.A. (2014) A Pre-  
490 dictive Model of the Dynamics of Body Weight and Food Intake in  
491 Rats Submitted to Caloric Restrictions. *PLOS ONE* 9(6): e100073.  
492 <https://doi.org/10.1371/journal.pone.0100073>
- 493 [12] Jo, J., Gavrilova, O., Pack, S., Jou, W., Mullen, S., et al. (2009). Hypertrophy  
494 and/or Hyperplasia: Dynamics of Adipose Tissue Growth. *PLOS Computational*  
495 *Biology* 5(3): e1000324. <https://doi.org/10.1371/journal.pcbi.1000324>
- 496 [13] Jo, J., Shreif, Z., Periwal, V. (2012). Quantitative dynamics of adipose cells.  
497 *Adipocyte*, 1(2), 80–88. <https://doi.org/10.4161/adip.19705>
- 498 [14] Jo J., Shreif Z., Gaillard J.R., Arroyo M., Cushman S.W., Periwal V. (2013).  
499 Mathematical Models of Adipose Tissue Dynamics. In: Gefen A., Benayahu  
500 D. (eds) *The Mechanobiology of Obesity and Related Diseases. Studies in*  
501 *Mechanobiology, Tissue Engineering and Biomaterials*, 16, Springer, Cham.  
502 [https://doi.org/10.1007/8415\\_2013\\_170](https://doi.org/10.1007/8415_2013_170)
- 503 [15] Li, Y., Periwal, V., Cushman, S. W., Stenkula, K. G. (2015). Adipose  
504 cell hypertrophy precedes the appearance of small adipocytes by 3 days in  
505 C57BL/6 mouse upon changing to a high fat diet. *Adipocyte*, 5(1), 81–87.  
506 <https://doi.org/10.1080/21623945.2015.1128588>
- 507 [16] Lönn, M., Mehlig, K., Bengtsson, C., Lissner, L. (2010). Adipocyte size predicts  
508 incidence of type 2 diabetes in women. *FASEB journal : official publication of*  
509 *the Federation of American Societies for Experimental Biology*, 24(1), 326–331.  
510 <https://doi.org/10.1096/fj.09-133058>
- 511 [17] MacKellar J., Cushman S.W., Periwal V. (2010) Waves of Adipose Tissue  
512 Growth in the Genetically Obese Zucker Fatty Rat. *PLoS ONE* 5(1): e8197.  
513 <https://doi.org/10.1371/journal.pone.0008197>
- 514 [18] McLaughlin, T., Sherman, A., Tsao, P., Gonzalez, O., Yee, G., Lamendola, C.,  
515 Reaven, G. M., Cushman, S. W. (2007). Enhanced proportion of small adipose  
516 cells in insulin-resistant vs insulin-sensitive obese individuals implicates impaired

- 517 adipogenesis. *Diabetologia*, 50(8), 1707–1715. [https://doi.org/10.1007/s00125-](https://doi.org/10.1007/s00125-007-0708-y)  
518 [007-0708-y](https://doi.org/10.1007/s00125-007-0708-y)
- 519 [19] Owen, A. B. (2020) On dropping the first Sobol’ point. arXiv:2008.08051 [cs,  
520 math, stat]. <http://arxiv.org/abs/2008.08051>.
- 521 [20] Saltelli A. (2002) Making best use of model evaluations to compute  
522 sensitivity indices, *Computer Physics Communications*, 145(2), 280–297.  
523 [https://doi.org/10.1016/S0010-4655\(02\)00280-1](https://doi.org/10.1016/S0010-4655(02)00280-1).
- 524 [21] Schlichting A. (2019). The Exchange-Driven Growth Model: Basic Prop-  
525 erties and Longtime Behavior. *Journal of Nonlinear Science* 30, 793–830.  
526 <https://doi.org/10.1007/s00332-019-09592-x>
- 527 [22] Skurk, T., Alberti-Huber, C., Herder, C., Hauner, H. (2007). Rela-  
528 tionship between adipocyte size and adipokine expression and secretion.  
529 *The Journal of clinical endocrinology and metabolism*, 92(3), 1023–1033.  
530 <https://doi.org/10.1210/jc.2006-1055>.
- 531 [23] Sobol’ I.M. (2001) Global sensitivity indices for nonlinear mathematical models  
532 and their Monte Carlo estimates, *Mathematics and Computers in Simulation*, 55  
533 (1?3), 271–280. [https://doi.org/10.1016/S0378-4754\(00\)00270-6](https://doi.org/10.1016/S0378-4754(00)00270-6).
- 534 [24] Soula, H.A., Julienne, H., Soulage, C.O., G elo en, A. (2013). Modelling  
535 adipocytes size distribution. *Journal of Theoretical Biology*, 332, 89–95.  
536 <https://doi.org/10.1016/j.jtbi.2013.04.025>
- 537 [25] Soula, H. A., G elo en, A., Soulage, C. O. (2015) Model of adipose tissue cellularity  
538 dynamics during food restriction. *Journal of theoretical biology*, 364, 189–196.  
539 <https://doi.org/10.1016/j.jtbi.2014.08.046>
- 540 [26] Toni T., Welch D., Strelkova N., Ipsen A., Stumpf M. P. (2009) Approximate  
541 Bayesian computation scheme for parameter inference and model selection in  
542 dynamical systems. *Journal of the Royal Society, Interface*, 6(31), 187?202.  
543 <https://doi.org/10.1098/rsif.2008.0172>
- 544 [27] Van Harmelen V., Skurk T., R ohrig K., Lee Y. M., Halbleib M., Aprath-  
545 Husmann I., and Hauner H. (2003). Effect of BMI and age on adipose tissue  
546 cellularity and differentiation capacity in women. *International journal of obe-*  
547 *sity and related metabolic disorders : journal of the International Association*  
548 *for the Study of Obesity*, 27(8), 889–895. <https://doi.org/10.1038/sj.ijo.0802314>
- 549 [28] <https://maple.cloud/app/6509768948056064>

550 [29] <https://github.com/CMA-ES/pycma>

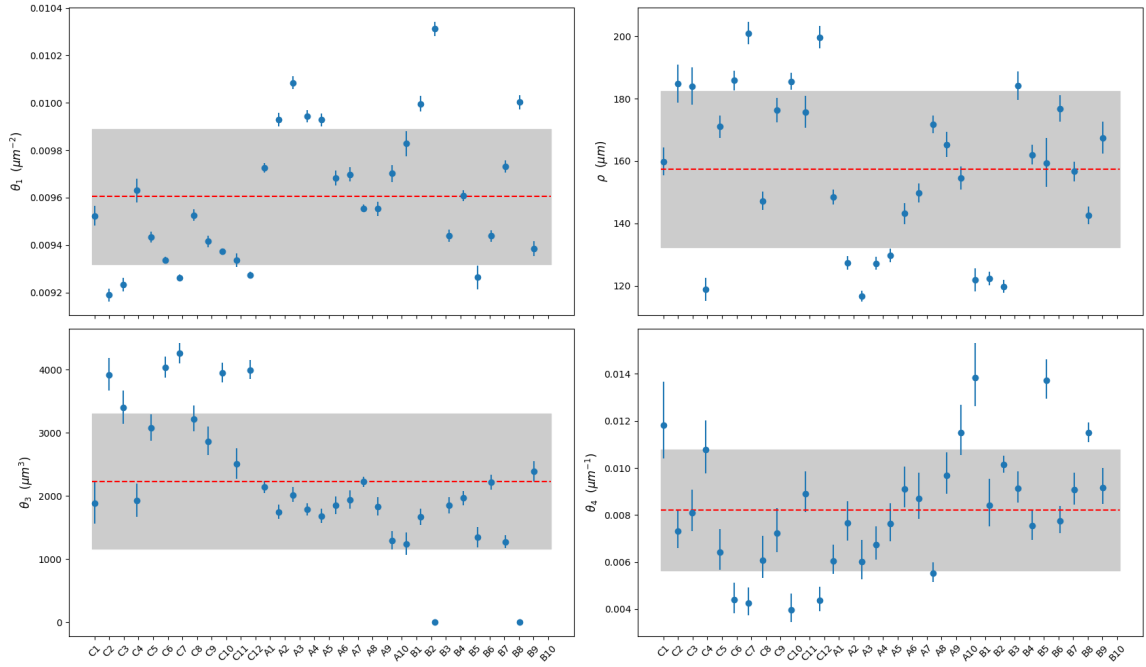


Figure 3: **Group variability and range of selected values.** Upper left and right figures display the results for parameters  $\theta_1$  and  $\rho$ . Lower left and right figures show the results for parameters  $\theta_3$  and  $\theta_4$ . For each estimated parameter the average over the population is shown with dash red line and the gray area is one standard deviation around the average computed over the population (values are reported in Table 4). For each parameter, the estimated value for each animal is displayed with dots and the bar represents the range of selected values. These ranges consist in values of the parameter (assuming the 3 others are fixed) for which the maximal cost function is 0.1% of the obtained cost function with the estimation (see section 3.2). All numerical values are reported in Table 5.



Table 5: **Parameter estimation results on measured adipocyte radius distribution in 32 rats.** First column is the animal identification. Estimation is performed with CMA-ES algorithm of `fmin2` function from `cma` Python package by minimizing the cost function  $\mathcal{L}$ , see eq. (18). The second to fourth columns show each parameter estimated value for each rat averaged over 100 runs with different initial guesses and the standard deviations are in brackets. For each estimated parameter, considering a maximum change of 20% of its estimated value, 1,000 samples are selected with a maximal error rate of 0.1% of the cost function value. The range of selected values of each parameter is given in the last four columns. These ranges consist in values of the parameter (assuming the other are fixed) for which the maximal cost function is 0.1% of the obtained cost function with the estimation. One can note that animals *B3* and *B9* have a value of  $\theta_3$  that is estimated to be zero ( $10^{-12}/10^{-13}$ ). Indeed, these animals show particular cell size distributions with a very large number of small cells which can be due to a measurement artifact.

animal	estimated values				selected ranges			
	$\theta_1 10^{-3}$ (std $10^{-11}$ )	$\rho 10^2$ (std $10^{-6}$ )	$\theta_3 10^3$ (std $10^{-4}$ )	$\theta_4 10^{-3}$ (std $10^{-10}$ )	$\theta_1 10^{-3}$	$\rho 10^2$	$\theta_3 10^3$	$\theta_4 10^{-3}$
C1	9.52 (3.12)	1.60 (2.94)	1.89 (2.31)	11.8 (7.95)	9.49 - 9.56	1.56 - 1.64	1.59 - 2.21	10.5 - 13.5
C2	9.19 (1.05)	1.85 (2.16)	3.92 (1.07)	7.31 (3.43)	9.17 - 9.21	1.79 - 1.90	3.70 - 4.16	6.67 - 8.10
C3	9.23 (1.33)	1.84 (2.54)	3.40 (1.50)	8.10 (4.82)	9.21 - 9.26	1.79 - 1.89	3.17 - 3.65	7.40 - 8.99
C4	9.63 (2.27)	1.19 (1.63)	1.92 (1.52)	10.8 (5.75)	9.59 - 9.68	1.15 - 1.22	1.70 - 2.16	9.88 - 11.9
C5	9.43 (1.75)	1.71 (1.99)	3.08 (1.34)	6.43 (3.25)	9.41 - 9.45	1.68 - 1.74	2.90 - 3.27	5.75 - 7.31
C6	9.34 (1.41)	1.86 (1.92)	4.04 (1.13)	4.39 (2.33)	9.32 - 9.35	1.83 - 1.89	3.89 - 4.19	3.88 - 5.08
C7	9.26 (1.02)	2.01 (1.89)	4.26 (0.91)	4.26 (2.02)	9.25 - 9.27	1.98 - 2.04	4.12 - 4.42	3.80 - 4.86
C8	9.53 (2.15)	1.47 (1.86)	3.22 (1.36)	6.09 (3.29)	9.50 - 9.55	1.45 - 1.50	3.04 - 3.41	5.42 - 7.01
C9	9.42 (1.9)	1.76 (2.25)	2.87 (1.49)	7.24 (3.65)	9.39 - 9.44	1.73 - 1.80	2.68 - 3.08	6.52 - 8.20
C10	9.37 (1.81)	1.86 (2.19)	3.95 (1.35)	3.97 (2.25)	9.36 - 9.39	1.83 - 1.88	3.81 - 4.10	3.50 - 4.58
C11	9.34 (1.69)	1.76 (2.46)	2.51 (1.81)	8.90 (5.35)	9.31 - 9.36	1.71 - 1.80	2.30 - 2.73	8.19 - 9.76
C12	9.27 (0.95)	2.00 (1.80)	4.00 (0.83)	4.37 (1.78)	9.26 - 9.29	1.96 - 2.03	3.87 - 4.14	3.98 - 4.89
A1	9.73 (1.5)	1.48 (1.04)	2.14 (0.60)	6.06 (1.77)	9.71 - 9.74	1.46 - 1.50	2.05 - 2.23	5.55 - 6.67
A2	9.93 (2.23)	1.27 (1.12)	1.75 (0.74)	7.65 (2.87)	9.90 - 9.96	1.25 - 1.29	1.65 - 1.85	6.98 - 8.50
A3	10.1 (2.76)	1.17 (1.01)	2.02 (0.79)	6.01 (2.48)	10.1 - 10.1	1.15 - 1.18	1.92 - 2.13	5.35 - 6.86
A4	9.94 (2.01)	1.27 (1.03)	1.79 (0.60)	6.74 (2.17)	9.92 - 9.97	1.25 - 1.29	1.70 - 1.88	6.18 - 7.44
A5	9.93 (1.91)	1.30 (1.05)	1.68 (0.63)	7.62 (2.58)	9.90 - 9.95	1.28 - 1.32	1.59 - 1.79	6.98 - 8.42
A6	9.68 (1.44)	1.43 (1.15)	1.85 (0.62)	9.11 (2.70)	9.65 - 9.71	1.40 - 1.46	1.73 - 1.98	8.41 - 9.97
A7	9.70 (1.81)	1.50 (1.38)	1.93 (0.75)	8.72 (3.22)	9.67 - 9.72	1.47 - 1.53	1.81 - 2.07	7.92 - 9.68
A8	9.55 (0.98)	1.72 (1.07)	2.23 (0.49)	5.53 (1.43)	9.54 - 9.57	1.69 - 1.74	2.16 - 2.30	5.20 - 5.94
A9	9.55 (1.54)	1.65 (1.66)	1.83 (0.78)	9.70 (3.63)	9.53 - 9.58	1.62 - 1.69	1.71 - 1.97	8.98 - 10.1
A10	9.70 (1.71)	1.54 (1.35)	1.3 (0.77)	11.5 (4.09)	9.67 - 9.74	1.51 - 1.58	1.17 - 1.44	10.5 - 12.6
B1	9.83 (2.16)	1.22 (1.36)	1.24 (0.94)	13.8 (6.65)	9.78 - 9.88	1.19 - 1.25	1.09 - 1.40	12.7 - 15.2
B2	10.0 (2.31)	1.22 (1.06)	1.67 (0.70)	8.42 (2.80)	9.97 - 10.0	1.20 - 1.24	1.56 - 1.79	7.61 - 9.45
B3	10.3 (1.42)	1.20 (0.74)	9.24 $10^{-16}$ (1.52 $10^{-8}$ )	10.1 (9.13)	10.3 - 10.3	1.18 - 1.22	0.76 - 1.09 $10^{-15}$	9.83 - 10.5
B4	9.44 (1.04)	1.84 (1.43)	1.85 (0.62)	9.14 (2.53)	9.41 - 9.46	1.80 - 1.88	1.74 - 1.97	8.60 - 9.81
B5	9.61 (1.16)	1.62 (1.06)	1.97 (0.61)	7.54 (2.35)	9.59 - 9.63	1.59 - 1.65	1.87 - 2.07	7.02 - 8.19
B6	9.26 (2.11)	1.59 (2.15)	1.34 (0.87)	13.7 (6.14)	9.22 - 9.31	1.52 - 1.67	1.21 - 1.49	13.0 - 14.5
B7	9.44 (0.93)	1.77 (1.2)	2.22 (0.55)	7.76 (2.44)	9.42 - 9.46	1.73 - 1.81	2.11 - 2.33	7.27 - 8.34
B8	9.73 (1.69)	1.57 (1.22)	1.28 (0.73)	9.07 (3.23)	9.71 - 9.76	1.54 - 1.59	1.19 - 1.37	8.51 - 9.72
B9	10 (1.17 $10^5$ )	1.43 (1.25 $10^5$ )	1.74 $10^{-6}$ (17.4)	11.5 (8.22 $10^4$ )	9.97 - 10.0	1.40 - 1.45	1.43 - 2.05 $10^{-6}$	11.1 - 11.9
B10	9.38 (1.52)	1.67 (1.98)	2.39 (0.81)	9.17 (3.68)	9.36 - 9.41	1.63 - 1.72	2.25 - 2.53	8.55 - 9.93

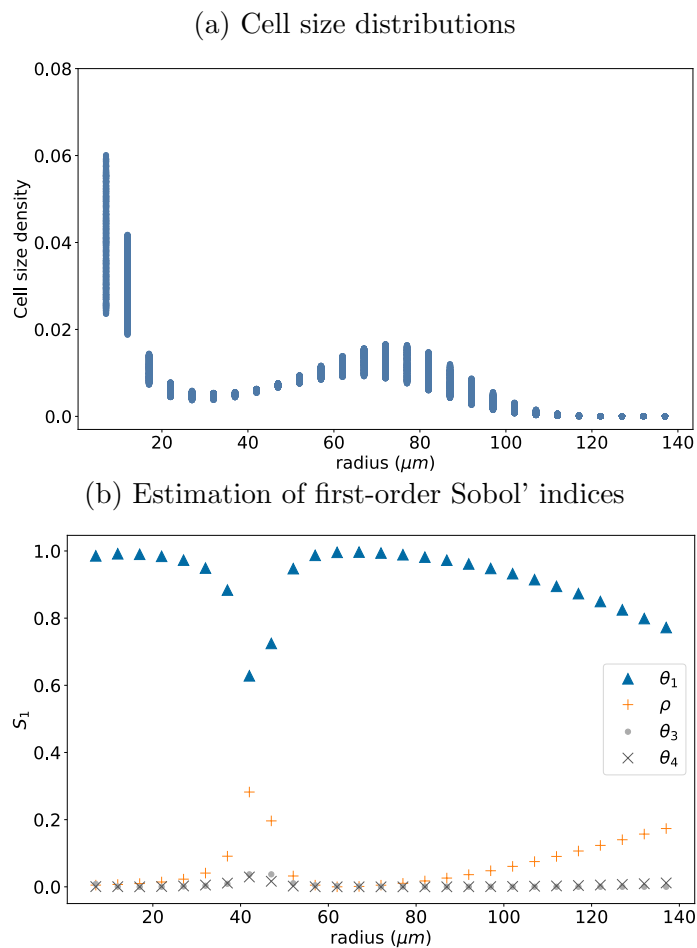


Figure 4: (a) A sample of cell size distributions. The parameter sampling design is constructed using Saltelli algorithm where each parameter is uniformly distributed in a range of values corresponding to  $\pm 1\%$  of the mean of its estimated value in rats (Table 4). A number of 20,480 samples giving bimodal distributions are generated to estimate the Sobol' indices. (b) Estimation of first-order Sobol' indices for  $\theta_1$ ,  $\rho$ ,  $\theta_3$  and  $\theta_4$  using a Monte-Carlo based approach [23, 20, 3, 19].